J. Phys. E: Sci. Instrum., Vol. 15, 1982. Printed in Great Britain

REVIEW ARTICLE

# Field-ion microscopy – A review of basic principles and selected applications

**J A Panitz**
Sandia National Laboratories, Surface Physics Division 114, Albuquerque, New Mexico 87185, USA

## 1. Introduction

'It seems as if the evasive atoms still hide from the curious eye of the casual sightseer and reveal themselves rewardingly only to the serious researcher' (Müller 1965). Although this quote by the inventor of the field-ion microscope may have accurately described the state of field-ion microscopy in 1965, today the low-temperature field-ion microscope (or FIM) provides a routine and simple way of investigating metal surfaces in atomic resolution. With only a modest investment in equipment the atoms which form the surface of a metallic solid can be imaged, and their movement charted as they are perturbed by subtle morphological and chemical changes occurring over ångstrom dimensions.

It is perhaps ironic that the FIM was introduced as late as 1950 since many of the concepts and techniques essential to its development had been perfected almost thirty years earlier (Eyring *et al* 1928). If a fluorescent material had been placed on the anode of their field-electron emission diode, the field-electron emission microscope – the precursor to the FIM – would have been available ten years earlier. If, in addition, a positive potential had been applied to their sharply curved specimen in a background of hydrogen gas (rather than in vacuum) the FIM might have been born. Instead, twenty-three years elapsed before the field-ion microscope became a reality (Müller 1951). For the first time, human beings could actually see individual atoms, a truly monumental accomplishment considering the simplicity of the technique.

The FIM achieves its magnification by almost radial projection of positive ions from the immediate vicinity of a sharply pointed specimen called a 'field-emitter tip'. The tip is usually prepared by simple electrochemical polishing techniques (Müller and Tsong 1969) from a wire which is typically less than a few tenths of a millimeter in diameter. Since the size of the tip apex is smaller than the size of individual crystallites in most polycrystalline materials, a tip prepared from polycrystalline wire will usually be formed from a single, perfect crystal. (Occasionally, a tip will be formed from two or more single crystallites of the polycrystalline wire separated by one or more well defined grain boundaries.) Figure 1 shows a transmission electron micrograph of a thermally annealed field-emitter tip viewed in profile.

As a result of the preparation technique, the surface of the tip apex will display many different crystal planes of low and high Miller indices, smoothly joined into an approximately hemispherical contour. This is seen in the ball model of figure 2 (Müller 1960) which depicts the apex of a field-emitter tip formed from a single BCC crystal. The close-packed (011) plane at the centre of the model corresponds to the orientation of the crystal along the wire axis. The large number of crystallographic orientations available for study on a single FIM specimen is one of the major advantages of the field-ion technique for surface studies.

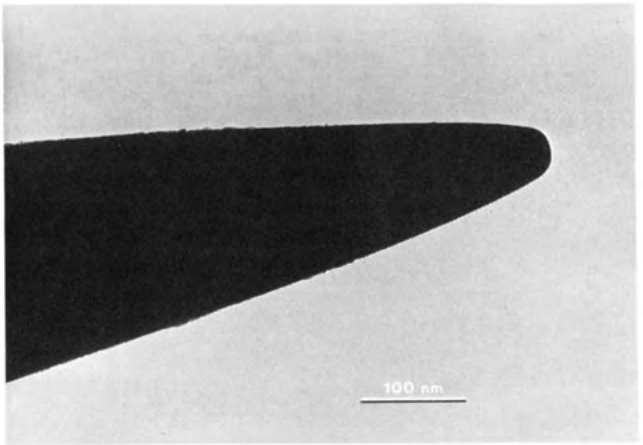


**Figure 1.** A transmission electron micrograph of a (011) oriented, tungsten field-emitter tip viewed in profile. A tip is usually prepared from polycrystalline wire, a few tenths of a millimetre in diameter. Its end is fabricated into an approximately spherical contour by chemical (or electrochemical) polishing techniques. After thermal annealing near its melting point, and/or high-field preparation, the tip apex is ready for imaging in the FIM.

As we will see, the field-ion imaging process is very sensitive to local variations in the electric field strength applied to the surface of the emitter tip. On an atomic scale, the field varies most strongly in the vicinity of exposed surface atoms which form the corner of abrupt lattice steps. As a result, a very good simulation of a FIM image can be obtained by highlighting these regions of the ball model with fluorescent paint and photographing the model in the dark. The result is shown in figure 3 where essentially all of the atoms having four next-nearest neighbours appear brightly illuminated (those atoms on adjacent less protruding sites appear more dimly). An FIM image of a (011) oriented tungsten tip is shown in figure 4 for comparison.

In order to index an actual FIM image it is helpful to compare

0022-3735/82/121281 + 14 $02.00 

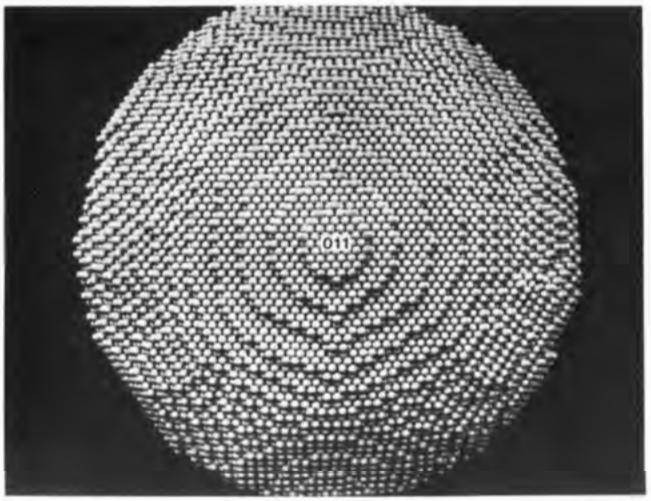


**Figure 2.** A cork ball model of the sharply pointed end of a (011) oriented, field-emitter tip. Lattice atoms form (011) net planes of increasing in diameter which form the nearly spherical contour of the tip apex. The radius of curvature of the tip apex depicted by the model is approximately 13 nm.

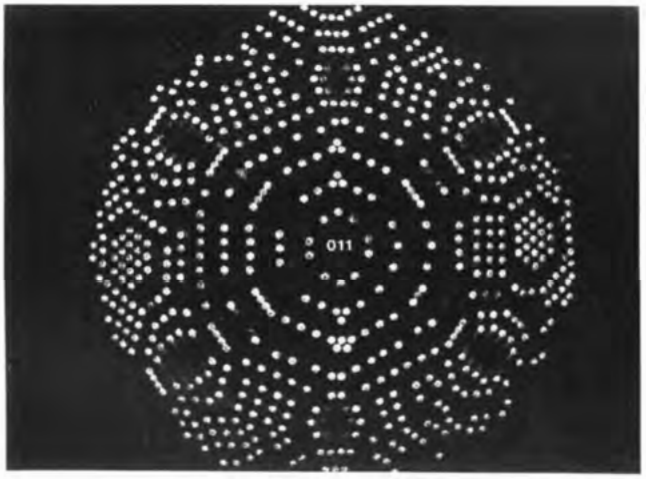


**Figure 3.** The cork ball model of figure 2 in which the most protruding and second most protruding atoms have been painted with a fluorescent dye. The model was photographed in the dark under ultraviolet illumination in order to highlight these atoms which are the ones which tend to be imaged in the FIM.

it to a ball model of the tip, and to the expected symmetry and surface structure of the lattice known from x-ray analysis. Although the relative positions of the various crystal planes depend to some extent on the shape of the emitter tip, it is usually sufficient to compare the image to an orthographic projection of a hemispherical crystal lattice. These are readily available (Müller and Tsong 1969, Müller 1960).

## 2. Image magnification

The FIM is a very simple microscope. Magnification is provided by radial projection of positive ions from the vicinity of the tip as shown schematically in figure 5. Because lenses are not used, the magnification of this 'point-projection' microscope is determined purely by geometric considerations. If a tip of radius

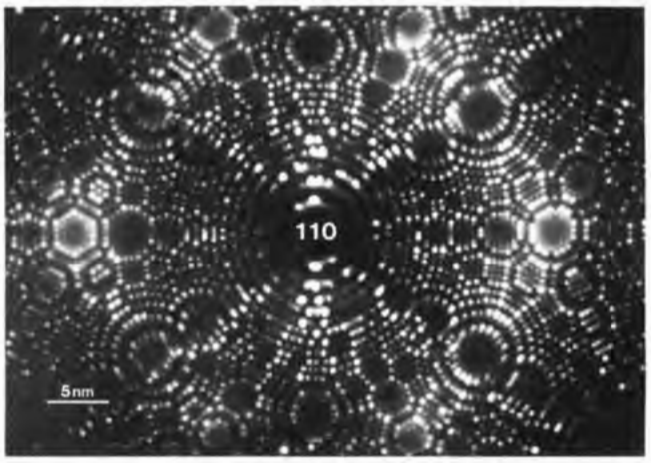


**Figure 4.** An FIM image of a (011) tungsten field-emitter tip. The tip was imaged in helium at 10 K using microchannel plate image intensification. (Figure courtesy of G D W Smith, The Department of Metallurgy and Material Sciences, University of Oxford, Oxford, England).

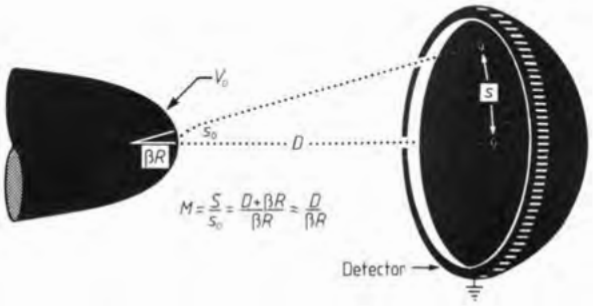


**Figure 5.** A schematic representation of the magnification process in the field-ion microscope. A specimen tip is biased to a positive potential, $V_0$. Ions formed in the vicinity of the tip apex are accelerated almost radially into space. If the trajectories from the tip are projected backward, they will tend to intersect within the tip, at a distance $\beta R$ from its surface; $\beta R$ can be treated as an effective tip radius. $R$ is the measured radius of the tip and $\beta$ is an 'image compression' factor. For an isolated sphere in space $\beta = 1.0$.

$R$ is placed a distance $D$ from a suitable ion detector, a reasonable estimate of the image magnification, $M$, will be given by

$$M = D/\beta R \qquad (1)$$

where $1.5 < \beta < 1.8$. Beta is an 'image compression factor' which accounts for any deviation in the ion trajectories from pure radial projection caused by the presence of the equipotential tip wire and its supporting assembly (Müller and Tsong 1969). Since a field-emitter tip can be etched to an apex radius of tens of nanometers, a magnification of several million times is easy to achieve. It is important to emphasise that the FIM imaging process does not utilise a *probing* beam of ions. As a result, the substrate cannot move relative to the imaging species, and external vibrations will not be magnified. This means that a magnification of several million times is useful in practice.

The actual magnification of a field-ion image will vary slightly across the imaged area because of local variations in the radius of curvature of the tip. Fortunately, a very precise, local magnification can be obtained directly from the image (Müller and Tsong 1969, Dreschler, 1960). The method is shown schematically in figure 6. If $\gamma$ is the known apex angle between two imaged, crystallographic directions, and $n$ is the number of net plane rings of known step height, $s$, which are resolved in the image, then the local radius of curvature is

$$R_L = ns/(1-\cos\gamma). \tag{2}$$

For cubic crystals, the step heights of the $\{hkl\}$ poles are given by

$$s = a/\delta(h^2+k^2+l^2)^{1/2} \tag{3}$$

where $a$ is the lattice constant and $\delta = 1$ or 2 as shown in table 1 (Müller and Tsong 1969). For tungsten, an average tip radius (in nanometers) can be obtained by multiplying the number of net plane rings seen in the image between the centres of the (011) and (121) planes by 0.16. Unlike an electron micrograph, each resolved field-ion image contains its own magnification standard which is the crystal lattice itself.

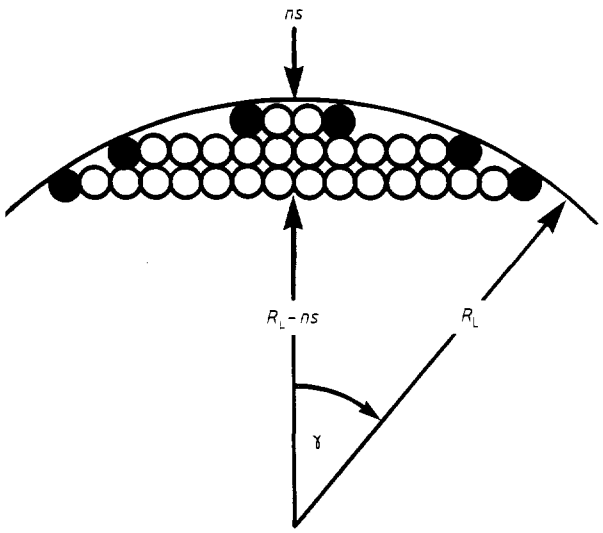


**Figure 6.** A schematic drawing of a tip in profile showing two crystallographic directions separated by a known angle, $\gamma$. $R_L$ is the local radius of curvature of the tip; $n$ is the number of net plane rings seen in the image and $s$ is the known step height per ring (see text). The dark edge atoms are those which are seen in an FIM image.

## 3. Imaging considerations

In theory, any mechanism which can create charged particles within a localised region of the tip surface can provide a point-projection imaging capability. As early as 1941, Müller deduced that barium ions were being created from a layer of barium atoms adsorbed on the tip surface whenever a positive electric field greater than 8 V nm$^{-1}$ was applied to the tip (Müller 1941). Müller later suggested that such a process could provide a magnified image of the adsorption sites of barium on the surface, provided individual barium ions could be detected (Müller 1951). The difficulty with such an imaging scheme is the very small ion currents which it produces. Even a monolayer of surface species producing positive ions from the entire imaged area of the tip would yield only $10^{-14}$ coulombs of charge.

**Table 1.** The scaling factor, $\delta$, used in equation (3) of the text to determine the step heights of the $hkl$ poles in a field-ion image.

| $\delta$ | Simple cubic lattice | BCC lattice | FCC lattice |
|---|---|---|---|
| 1 | All values of $h, k, l$ | $h+k+l$, even | $h, k, l$ odd |
| 2 | | $h+k+l$, odd | $h, k, l$ mixed parity |

Müller reasoned that for a barely discernible image on a fluorescent screen, an image intensification of at least $10^6$ would be required (Müller 1951). Since modern image intensifiers were not available at the time, this could only be accomplished by a rapid succession of individual, adsorption–desorption sequences, with the resulting images photographically integrated. A convenient approach would involve supplying the imaging species from the gas phase so that a continuous coverage of surface species would be available for desorption. This, in fact, seems to be the rationale which led Müller to the first operating FIM. Hydrogen was selected for an imaging species and introduced into an existing field-electron microscope (Müller 1936a, b) by diffusion through a heated palladium tube (Müller 1951). Müller believed that if a room temperature emitter tip was kept at a sufficiently high positive bias in the presence of ambient hydrogen, an adsorption–desorption cycle could be indefinitely maintained. We now know that field-ionisation of gas phase hydrogen (rather than desorbed, surface hydrogen) was responsible for the images which were observed. But, fortuitously, the right conditions were established, and a truly revolutionary microscope was born.

## 4. Field ionisation

Field ionisation of an isolated atom in free space by electron tunnelling was first proposed by Oppenheimer (Oppenheimer 1928). By formulating the problem quantum mechanically, he was able to demonstrate that the lifetime of an electron in an isolated hydrogen atom depended upon the magnitude of an external electric field. At fields of the order of 0.1 V mm$^{-1}$, the calculated lifetime ($\approx 10^{100}$ yrs) was greater than the expected age of the universe, but at fields approaching 25 V nm$^{-1}$, ionisation would occur within a small fraction of a second (Inghram and Gomer 1956). Although it seemed to be impossible to create a positive field strength of this order of magnitude Eyring, Mackeown and Millikan were able to obtain a positive field of about 10 V nm$^{-1}$ in a high-vacuum environment (Eyring *et al* 1928).

In 1931, Lanczos suggested that field-induced quenching of spectral lines in the Stark effect could be explained by quantum mechanical tunnelling from an excited state of the hydrogen atom (Lanczos 1931). Guerney thought that the tunnelling process could also explain the neutralisation of hydrogen ions at the cathode of an electrolytic cell (Guerney 1932). He further noted that tunnelling should occur at a critical distance from the electrode surface where the ground state energy of the atom was equal to the Fermi level of the metal. However, the field-ion imaging process was not satisfactorily explained until Inghram and Gomer presented a theoretical model of field ionisation in the vicinity of a metal surface (Inghram and Gomer 1954). Their description of the process indicated that field-ion images are produced by continuous, gas phase ionisation and not by an adsorption–desorption cycle at the tip surface.

In free space, the valence electron of a neutral atom can be

considered as bound in a potential well. The depth of the well is equal to the potential of the atom, $I$. In an electric field, the potential well will be distorted, and the probability for tunnelling into the vacuum will increase. As the electric field strength is raised, the width of the potential barrier which the electron 'sees' will become comparable to its de Broglie wavelength. Consequently, the probability for tunnelling through the barrier will greatly increase. If the atom is close to a metal surface, the barrier width will decrease further, due to short-range contributions to the potential from atom–surface interactions (Müller and Tsong 1973).

Since tunnelling can occur only into an unoccupied state of the metal, the probability of tunnelling will be appreciable only if the ground state of the valence electron in the atom lies above the Fermi level of the metal. This condition (shown schematically in figure 7) is satisfied at some critical distance, $X_c$, from the metal surface such that

$$eFX_c = I - \Phi \tag{4}$$

where $F$ is the field strength and $\Phi$ is the workfunction of the metal.

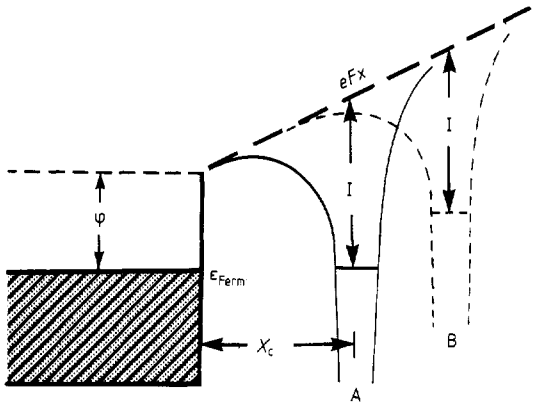


**Figure 7.** A schematic drawing of the field-ionisation process near a metal surface having a workfunction, $\Phi$. At position A the atom is located a distance $X_c$ from the metal surface. $X_c$ is the critical distance for field-ionisation, and corresponds to the position at which the energy level of the valence electron in the atom is equal to the Fermi energy of the metal. At closer distances to the surface (within the so-called 'forbidden zone') the energy level of the electron will lie below the Fermi energy and the tunnelling probability will be low. At increasing distances from the surface (position B), the barrier width will become larger and the tunnelling probability will decrease.

The image potential due to the tunnelling electron (and the change in the polarisation energy of the atom upon ionisation) have been omitted in equation (4) because their combined contribution is usually negligible. For hydrogen, $I = 13.5$ eV. In its ionisation field of 25 V nm$^{-1}$ above a tungsten surface, (where $\Phi \approx 4.5$ eV) the critical distance for ionisation, $X_c \approx 0.4$ nm.

A reasonably accurate estimate of the ionisation probability of an atom at the critical distance can be obtained by multiplying the probability of an electron tunnelling from the atom by the frequency with which it strikes the tunnelling barrier. The former can be estimated from the WKB approximation using a simplified triangular barrier (Müller and Tsong 1969). The latter can be estimated from the Bohr model using an 'effective' nuclear charge appropriate to the atom in question (Müller and Tsong 1969). The measured field-ion current should then be the product of the ionisation probability of an atom (assumed to be isotropic) and the number of atoms which arrive in the ionisation zone each second. The measured field-ion current is at least an order of magnitude larger than expected if it is assumed that the supply of imaging gas molecules is governed by the kinetic theory of gases, and the ionisation probability is 100%. The experimental observations were explained when it was realised that the number of gas phase molecules in the vicinity of the tip is artificially enhanced by field-induced dipole attraction to the tip apex. Imaging gas atoms having a polarisability, $\alpha$, will be polarised in the inhomogeneous field, $F$, above the tip apex. Including the enhancement factor due to the field-induced dipole energy, $\alpha F^2/2$ produced good agreement with the measured field-ion currents (Müller 1960, Inghram and Gomer 1955, Müller and Bahadur 1956).

## 5. Field-ion energy distributions

The energy distribution of field-ionised gas atoms above a tip surface can provide valuable insight into the nature of the field ionisation process. If an ion is created at the tip surface, it will acquire a kinetic energy corresponding to its acceleration through the full potential difference which is applied between the tip and a collector. If the ion is created in space at some distance from the surface, it will acquire less kinetic energy. As a result, the threshold energy in the energy distribution of field-ionised gas atoms will indicate the position at which the ions are formed, and the width of the distribution will reflect the spatial extent of the ionisation region above the tip surface.

The first energy distribution of field-ionised gas atoms was measured in 1954 by Inghram and Gomer using a magnetic sector mass spectrometer which incorporated a field-ionisation source (Inghram and Gomer 1954). With a better energy analyser, Müller and Bahadur found that the half-width of the energy distribution for field-ionised argon was $\approx 2$ eV, with a sharp threshold indicating spatial ionisation $\approx 0.05$ nm above the tip surface (Müller and Bahadur 1955, 1956). These measurements were confirmed and extended by Tsong and Müller to include a number of other gases including helium (Tsong and Müller 1964). The width of the helium distribution at 20 kV (corresponding to a field of 45 V nm$^{-1}$ and the best visual image) indicates that the region of ionisation is less than 0.02 nm thick. Since individual atoms are resolved in the field-ion image, the ionisation zone must also be laterally localised to a region of space directly above each protruding surface atom (where the electric field is greatest). As the field strength is increased, the field-ion image becomes blurred and the energy distribution broadens toward lower energies, indicating spatial ionisation further from the tip surface.

Additional insight into the nature of the ionisation process was provided by Jason, Burns and Inghram who discovered a weak, periodic structure in the low-energy tail of hydrogen and neon distributions (Jason *et al* 1965). Jason, and Aiferieff and Duke qualitatively explained the phenomena in terms of a resonance associated with the tunnelling of an electron between the ionising atom and the nearby metal surface (Jason 1967, Aiferieff and Duke 1967). In principle, the 'Jason effect' should depend critically on the morphology of the tip surface. Consider an electron which tunnels from a gas phase atom during the ionisation process. The electron will have a finite probability of being reflected from the nearby metal surface, but essentially a zero probability of tunnelling back into the resulting ion. Under such conditions, standing waves will exist in the potential well defined by the ionising atom and the metal surface. The strength of the resulting resonances (which manifest themselves in the

energy distribution as multiple Jason peaks) will depend upon the uniformity of the surface potential since it ultimately governs the electron reflectivity at the metal surface. The smoother the surface, the more uniform the potential, and the greater the probability for electron reflection. Müller and Krishnaswamy were able to confirm this intuitive picture by measuring field-ion energy distributions associated with individual atoms imaged in the field-ion microscope (Müller and Krishnaswamy 1973). (Jason had observed the effect in energy distributions averaged over the entire imaged area of tip.) As many as seven Jason peaks were found above the atoms of the close packed planes of tungsten and iridium, but only two or three above the more open 'structured' planes (such as the (111)). For highly disordered surfaces of carbon and silicon, multiple peaks were never detected.

At very high field strengths (above 50 V $nm^{-1}$) Müller and Krishnaswamy also found that a few per cent of the field-ionised noble gas atoms had energies higher than the threshold energy of the distribution. It appeared that some imaging gas molecules could ionise within the critical distance for field-ionisation given by equation (4). To explain the observation of ionisation within the so-called 'forbidden zone', they reasoned that a continuous current of low-energy electrons was bombarding the tip surface. These electrons were created by spatial ionisation of imaging gas atoms far from the tip. The electrons which struck the tip surface would have sufficient energy to raise the valence level of adsorbed imaging gas atoms above the Fermi energy of the metal. These atoms would then have a high probability of ionising.

Four years earlier, in 1969, Müller, McLane and Panitz had discovered that nobel gas atoms were bonded to the tip surface during imaging by a short-range, field-induced, dipole–dipole bond (Müller *et al* 1969). They called this unique type of bonding 'field-adsorption'. It provided a new picture of the imaging process. Previously, the high electric field strength required for imaging was thought to ionise all gas phase species in space, thereby keeping the tip surface free of gas phase contaminants. It is now known that during imaging, inert imaging gas molecules (and perhaps, hydrogen) are field-adsobed onto the tip surface in regions where the electric field strength is locally enhanced. In effect, an FIM tip acts as a reversible getter for polarisable gas phase species. During imaging, the number of these species bound to the tip surface will greatly increase. When the field is removed, the surface concentration will immediately revert to its zero-field, equilibrium value.

## 6. The hopping gas model

At a certain electric field strength (called the 'best-image' field), the field-ion image displays maximum surface detail and definition over the widest field of view (Müller and Tsong 1969). The best-image field is established by applying an empirically determined potential to the emitter tip which is called the 'best-image voltage' or BIV. Although BIV is a subjective parameter, different observers always choose the same BIV to within a few per cent. At BIV, field-ion energy distributions demonstrate that gas phase atoms are ionised in a volume of space which is less than 0.05 mm thick, and localised above the most protruding atoms of the tip surface.

As mentioned previously, imaging gas molecules having a polarisability, $\alpha$, will be polarised in the inhomogeneous field, $F$, above the emitter surface. As a result, they will strike the emitter tip at temperature, $T$, with a field-induced dipole energy, $1/2\alpha F^2 \gg kT$. If they do not condense on the tip surface, they will lose some fraction of this energy (determined by their thermal accommodation coefficient) and rebound, only to be attracted to the tip surface once again by polarisation forces. Since a reasonable fraction of the emitter tip apex is covered with field-adsorbed imaging gas molecules at BIV, the thermal accommodation process will be greatly enhanced.

One can picture the polarised gas-phase molecules as eventually being trapped in a region of space close to the emitter apex; losing energy by thermal accommodation to the temperature of the tip, and slowly diffusing over the tip surface in a random 'hopping' motion (Müller and Tsong 1969). During this process, each molecule will pass through the region of high ionisation probability above a protruding atom of the surface. If its velocity is sufficiently reduced by the thermal accommodation process, it will dwell in the ionisation region and have a high probability of losing an electron to the metal surface by the tunnelling process. The tunnelling probability is enhanced by the presence of field-adsorbed gas atoms at protruding sites directly below the ionisation region (Müller and Tsong 1973).

If tunnelling occurs, the positive ion will accelerate rapidly away from the tip surface in an almost radial direction. At an imaging gas pressure of several mTorr, some $10^5$ ions/sec are created above each protruding surface atom. This corresponds to an ion current of the order of $10^{-14}$ A. As a result, the intensity of a field-ion image on a fluorescent screen is roughly equivalent to that of the Milky Way, viewed with dark-adapted eyes, on a moonless night.

## 7. Image resolution

By hopping over the tip surface an imaging gas species will thermally accommodate to the temperature of the tip, $T$, and lose its field-induced dipole energy. After ionisation, the kinetic energy of the ion parallel to the tip surface will be of the order of $kT$. Since dipole energies are typically at least an order of magnitude larger than $kT$, the process of thermal accommodation is extremely important in determining the kinetic energy of the ion parallel to the tip surface. This, in turn, is important because it will be the largest contributing factor to the resolution of the FIM.

The resolution of the FIM is determined by the spread in the kinetic energy of the imaging gas ions parallel to the tip surface, the spatial extent of the ionisation zone, $\delta_0$, and diffraction effects due to the finite de Broglie wavelength of the ion. Since the latter effect is small compared to $\delta_0$, the resolution of the FIM, $\delta$, can be shown to be

$$\delta = \delta_0 + A(RT/F)^{1/2} \tag{5}$$

where $A$ is a constant, $R$ is the tip radius, $T$ is the tip temperature and $F$ is the imaging field (Müller and Tsong 1969). All things being equal, cooling the tip to cryogenic temperatures will make the most noticeable improvement in image resolution. For example, cooling the tip from room temperature to liquid nitrogen temperature should improve the image resolution by a factor of $(80/300)^{1/2} \approx 50\%$.

When the FIM was introduced, Müller mentioned that '... experiments were in progress with ... strongly cooled tips' (Müller 1951). But one year later, Gomer reported that immersing an entire FIM in liquid nitrogen did not improve the resolution of the image (Gomer 1952). Apparently, observing the FIM pattern through the glass walls of a liquid nitrogen dewar prevented an improvement in resolution from being noticed. Several years later, low-temperature imaging was again attempted in Erwin Müller's laboratory (Müller 1956a, b). Truly spectacular images of metallic surfaces were obtained in atomic resolution by the simple experimental procedure of cooling only the specimen tip to 80 K.

For optimum resolution at any tip radius, equation (5) predicts that the tip temperature should be kept as low as possible, and the electric field at BIV should be made as large as possible. Since the spatial extent of the ionisation region cannot

be better than the diameter of the atom used as an imaging gas, small imaging gas species which do not condense onto the tip surface are preferred. With a condensation temperature below 5 K, an effective diameter of 0.19 nm, and a best-image field of 45 V $nm^{-1}$, helium is by far the best choice for an imaging gas. Unfortunately, the mechanical stress exerted on the emitter by the field at helium BIV ($\varepsilon_0 F^2/2 \approx 10^{10}$ N $m^{-2}$) will elastically deform most materials. Only those materials which have a relatively high Young's modulus, and are free of major lattice defects will survive.

Refractory metals are particularly good candidates for field-ion imaging in helium. For example, figure 8 shows an iridium overlayer deposited onto W(110). The overlayer has a rhombohedral shape and a unit cell with the same symmetry as the underlying tungsten lattice (Fink and Ehrlich 1981). Figure 9 shows a silicon adlayer on W(110) formed by thermal equilibration of vapour-deposited silicon atoms (Tsong and Casanova 1981). Computer simulation of the expected equilibrium superstructure (based on pair potentials derived from FIM mesurements) are in excellent agreement with the experimental observations.

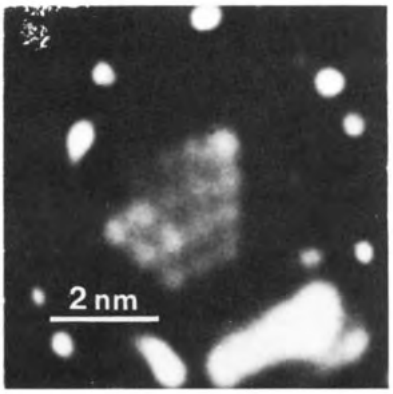


**Figure 8.** A cluster of sixteen iridium atoms which form an overlayer on W(110), equilibrated at a tip temperature of 460 K. (Figure courtesy of G Ehrlich, the Coordinated Science Laboratory, The University of Illinois at Urbana Champaign). Estimated micron marker error ±0.05 nm.

Other imaging gases or gas mixtures can often be used to reduce the field required for imaging and the field stress at BIV. For example, imaging in hydrogen occurs at about one-half of helium BIV, reducing the field stress by almost 50%. Frequently, a mixture of imaging gases will improve image contrast and resolution. Figure 10 shows a reconstructed tungsten (001) plane imaged in a helium–10% neon mixture below 20 K (Tung *et al* 1982). The image shows a perfect C(2 × 2) ($\sqrt{2} \times \sqrt{2}$) R45° domain consisting of nineteen atoms. Reconstruction was induced by field-evaporating a nearly perfect, unreconstructed (001) plane at 430 K. Since the FIM is the only instrument that can determine morphological changes on a surface in atomic resolution, it is ideally suited for studying adlayer structures on perfect crystal planes, surface rearrangement, and surface reconstruction.

One note of caution is in order. Reconstruction seen in FIM images may be difficult to correlate with zero-field observations because the field (or adsorbed imaging gas atoms) may tend to stabilise a particular configuration of atoms. Nevertheless, recent FIM studies have been productive, and may yield new insights into the reconstruction process (Melmed *et al* 1979).

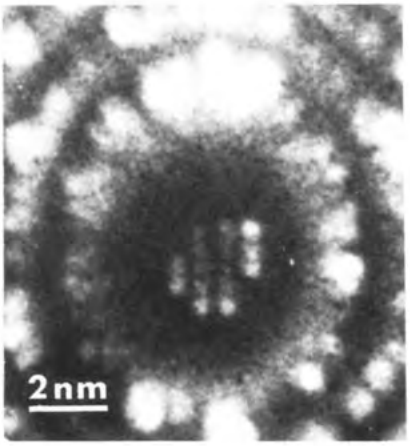


**Figure 9.** A helium-ion micrograph of a silicon adlayer on W(110) after annealing at 300 K for 50 s. (Figure courtesy of T T Tsong, The Field-Emission Laboratory, The Pennsylvania State University, University Park, Pennsylvania).

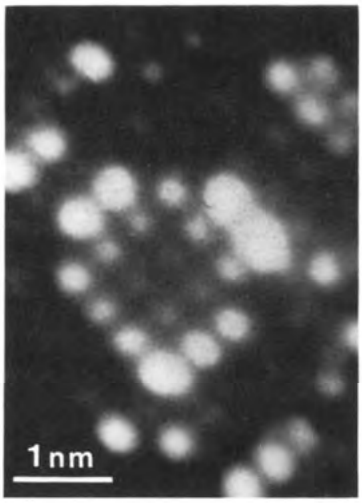


**Figure 10.** A perfect, single C(2 × 2), ($\sqrt{2} \times \sqrt{2}$) R45° domain containing 19 atoms, resulting from field-evaporation of a nearly perfect tungsten (001) plane at 430 K. The image was taken in a mixture of helium–10% neon below 20 K. (Figure courtesy of W R Graham, The Laboratory for Research on the Structure of Matter, The University of Pennsylvania, Philadelphia, Pennsylvania). Estimated micron marker error ±0.05 nm.

By a careful choice of imaging conditions a wide range of materials can be successfully imaged in the FIM. These include most of the metals in the periodic table (Müller and Tsong 1969); many alloys and semiconductors (Melmed and Stein 1975), and even insulators if they are first coated with a thin metallic layer in order to establish an imaging field at their apex (Walko 1982). In principle, tips made of insulating material could also be imaged by depositing charge directly onto their apex from an external source. If the tip apex is approximated by an isolated sphere of radius, $R$, and, a charge, $Q$, is deposited in order to produce an electric field strength, $F$, at its surface; then

$$Q = 4\pi\varepsilon_0 F R^2. \tag{6}$$

(See, for example, Feynman *et al* 1964). At helium BIV,

$F = 45$ V/nm. For a tip radius of 50 nm, $Q \approx 10^{-14}$ C which is equivalent to only $10^5$ electronic charges.

If the tip voltage is raised beyond BIV, the ionisation region in front of the tip will extend further into space and will become laterally delocalised. The FIM image will blur and lose resolution. As the electric field strength is further increased it will reach a value sufficiently high to ionise weakly bound surface species and displaced lattice atoms. These will be removed from the surface as positive ions. Eventually, even the lattice will begin to dissolve as lattice species become ionised. If the tip potential is held constant during this process, the tip surface will eventually assume a stable and nearly hemispherical contour, or 'endform', of minimum free energy. The surface will be atomically smooth, and can be as crystallographically perfect as the bulk lattice. By this process, clean surfaces can be routinely prepared with the atomic regularity required for high-resolution lattice imaging.

Once a stable endform is reached, the tip voltage can be lowered to BIV for imaging, or can again be increased in order to controllably dissect the near-surface region of the lattice, atomic layer by atomic layer. Since the lattice dissolves at high field strengths, bulk artefacts (naturally occurring in the near-surface region or purposely introduced) can be exposed for imaging. A particularly striking example of the power of this technique is shown in figure 11. A series of field-ion images were taken at successively higher field strengths exposing a small, coherent precipitate in a copper–1.7 at% iron alloy tip. Although not all FIM images of alloys are this well resolved, many can still yield useful information about particle size distribution and the extent of the precipitate-free zone which may surround them. At this level of resolution, the FIM is the only microscope capable of making such measurements.

## 8. Field evaporation

The removal of lattice atoms in a high electric field is called 'field-evaporation', by analogy with thermal evaporation at high temperatures and zero field (Müller 1956c). If the surface atoms are adsorbates, the process is called 'field-desorption'. Field-evaporation is usually considered to be a special case of the field-desorption phenomenon although, theoretically, there is no difference between the two. It is beyond the scope of this review to discuss the theory of field-evaporation. There is a long history of attempts to understand the process in detail (Müller and Tsong 1973, Gomer 1959, Gomer and Swanson 1963, Swanson and Gomer 1963, Brandon 1966a, b, 1965, Tsong 1968, Tsong and Müller 1970, Tsong 1971a, McKinstry 1972). Recently, a new insight has been provided by the theoretical and experimental work of Ernst (1979), by a new theoretical analysis by Haydock and Kingman (1980), and by Kellogg's unique experimental observations (Kellogg 1981, 1982a).

Mass spectrometric measurements demonstrated quite early that most metals field-evaporated as a double-charged ion at cryogenic temperatures (Barofsky and Müller 1968). Many evaporated in the triply charged state, and some even showed an appreciable abundance of quadruply charged ions (Müller and Tsong 1973). Charge states as high as +6 have been reported, but their abundance appears to be vanishingly small (Müller and Krishnaswamy 1976). As the temperature of the tip is raised, the

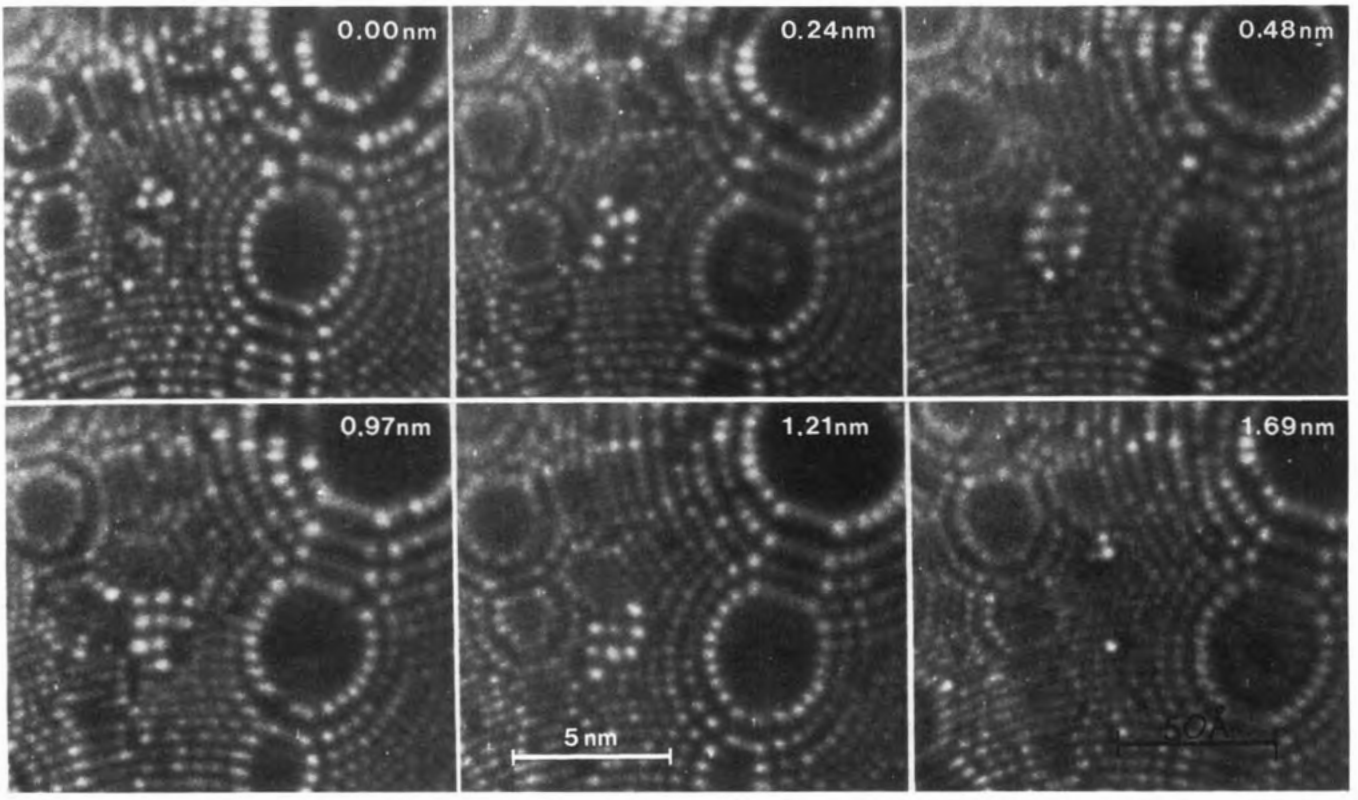


**Figure 11.** A sequence of FIM images taken as successively higher field strengths were used to expose a coherent precipitate in a Cu–1.7 at.% Fe tip heated for one hour at 500 °C. The depth probed into the lattice between each successive image is indicated in the upper right hand corner of each image. (Figure courtesy of S S Brenner, The United States Steel Corporate Research Laboratory, Monroeville, Pennsylvania.)

charge distribution of field-evaporated ions shifts to lower charge states, with singly charged ions dominating the mass spectra of most materials above room temperature (Müller and Tsong 1973). The problem with interpreting these measurements has been the inseparability of field and temperature effects. Field-evaporation is known to be a thermally activated process (Müller and Tsong 1969). If the tip temperature is increased, the electric field required to produce a given field-evaporation rate will be reduced. As a result, field and temperature are not independent parameters, but jointly contribute to the shift of the charge state distributions. Recently, Kellogg has shown that at least over a limited field range, it is possible to vary the two parameters independently (Kellogg 1981, 1982a). His measurements indicate that for a number of metals (and silicon), the field strength *and not the temperature* is actually responsible for the shift in the charge state distribution.

The relative abundance of the charge states which Kellogg measures (at constant temperature and increasing field strength) is in excellent agreement with Haydock and Kingman's three-dimensional tunnelling calculation (Haydock and Kingman 1980). It appears that surface species are initially removed as singly charged ions which have a finite probability of successively ionising to higher charge states in the field above the tip surface. The probability of multiple ionisation (or post-ionisation) depends upon the magnitude of the electric field strength since the field determines the width of the tunnelling barrier. It is reasonable to expect that thermal activation over a field-reduced energy barrier usually produces the initial ion, although at very low temperatures tunnelling may predominate (Müller and Tsong 1973). In fact, Müller's early 'image-force' theory of field-evaporation embodied the thermal activation concept, and has been reasonably successful in predicting the observed evaporation fields for species which form singly and doubly charged ions (Müller 1956c). Although this simple theory depends in detail upon the nature of the potential barrier at the surface, its basic concept – a neutral species thermally subliming from the tip surface and then ionising at the critical distance – is probably correct.

Neither the image force model, nor the post-ionisation refinement predict the crystallographic variation in abundance observed for many species (Panitz 1975a, b, Krishnaswamy and Müller 1977). Since the electric field strength determines the probability of post-ionisation, local crystallographic variations in the abundance of the higher charge states of refractory metals may just reflect local variations in the field-strength over the tip surface (Panitz 1975a). It is clear that the local field strength will be affected by the local morphology of the tip, and its local radius of curvature. However, more subtle effects, such as adsorbate coverage may also be important. This seems to be particularly true of hydrogen which is invisible in the field-ion image, but can appreciably reduce the local evaporation field (presumably by weakening the metal-to-metal bond at the surface). It is interesting to note that lattice hydrides are commonly observed in the mass spectra of field evaporating metals even if stable hydrides do not exist in the absence of a field (Krishnaswamy and Müller 1977).

## 9. The field-desorption microscope

The field-ion microscope provides a nondestructive image of a surface, in atomic resolution, by mapping variations in ionisation probability directly above protruding surface atoms. Gas phase species ionised in space above the tip surface probe subtle modulations in the electric field produced when moderate potentials are applied. A one-to-one correspondence between ionisation probability, local field-strength, and surface morphology allow an FIM image to be interpreted in terms of the individual atoms which constitute the outermost layer of the lattice.

A more direct imaging procedure would map the relative positions of individual surface species produced during a field-desorption event. By repetitively desorbing a weakly bound species, the surface of the tip would not be altered. Müller originally proposed using barium for this purpose (Müller 1941), and later with Bahadur, attempted to use nitrogen (Müller and Bahadur 1956). Both attempts failed, probably because image intensification was not available. In the latter case, field-induced corrosion would probably change the morphology of the tip surface during imaging so that reproducible images might have never been achieved. Recently, Kellogg and Tsong have shown that weakly bound, field-adsorbed helium which is present on the surface during normal FIM imaging can be used for imaging (Kellogg and Tsong 1981). Desorbing this species produces images which closely resemble a conventional field-ion image of the surface. This is not surprising since the field-ionisation process probes the position of surface atoms where the probability of field-adsorbing helium is also highest.

Another approach to image the lattice was advanced by George in 1965 (George 1965). He attempted to record the relative position of lattice atoms by using a three-stage image intensifier to observe the field-evaporation process in progress. Although a few scintillations above random background noise were recorded, no discernable image was seen. Until a microchannel plate image intensifier was placed within an operating field-ion microscope (Turner *et al* 1969), field-desorption imaging was not a practical technique. With this device, the desorption microscope became a reality (Walko and Müller 1972). Field-ion microscopy was no longer a tedious discipline restricted to metals which remained unchanged during a typical imaging period of twenty minutes.

## 10. Microchannel plate image intensification

A microchannel plate (or MCP) is composed of a myriad of glass capillaries arranged in an ordered array which is produced by selectively etching a fibre optic bundle (Lampton 1981). The plate, which can have a diameter of many centimetres, is usually about 1.5 mm thick and can be planar or spherically curved. A planar MCP viewed normal to its surface in an optical microscope is shown in figure 12. The capillary tubes are typically less than 40 $\mu$m in diameter, and are usually spaced on 50 $\mu$m centres. Each capillary acts as an individual electron multiplier when a potential difference of several hundred volts is applied to a conductive coating deposited on opposite sides of the plate. Incoming ions (or electrons) which strike a capillary wall produce, on the average, more than one secondary electron. These electrons are propagated through the channel by the electric field produced by the applied potential. Since electrons collide with the capillary wall several times during transit, an electron avalanche results. One electron striking the entrance to a capillary can easily produce a thousand electrons at its end. By properly biasing the front surface of the MCP, ions which strike the intercapillary area between adjacent channels can also be collected (Panitz and Foesch 1976).

The secondary electrons which emerge from each channel of a MCP are usually focused, electrostatically onto a phosphor coated plate where they produce a visible spot of light. If a field-ion image has sufficient magnification so that the ions from adjacent surface species are separated at the MCP by several channel diameters, individual ion impacts will be recorded, and an entire, weak, field-ion image will be visible in ambient room light. By cascading two microchannel plates in tandem, a gain of $10^6$ can be achieved. With this detector, images of individual, field-desorbed ions can be obtained.

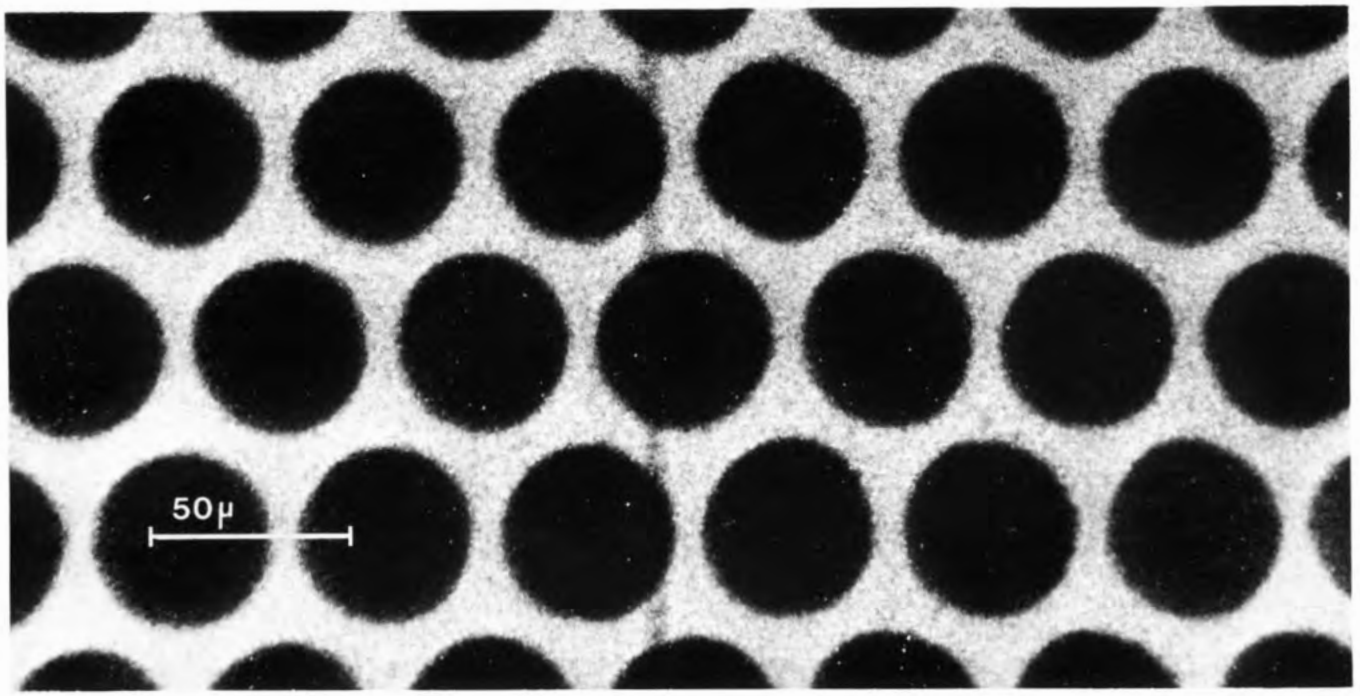


**Figure 12.** An optical micrograph of the central region of a microchannel plate, or 'MCP', which is also known as a CEMA (channel electron multiplier array). Each dark circular area is the entrance to a microcapillary tube which is typically 40 $\mu$m in diameter. Each capillary acts as an individual electron multiplier when a potential difference of several hundred volts is applied across the plate. A CEMA provides a convenient way to intensify a weak field-ion image when combined with a proximity focused fluorescent screen (see text).

The widespread use of a microchannel plate within a field-ion microscope has greatly extended its utility. Previously, many materials of interest could not be imaged in the FIM because their lattice field-evaporated before BIV was reached. With internal MCP detectors, materials which slowly field evaporate during imaging can be photographed because exposure times less than a tenth of a second are usually adequate.

### 11. The modern field-ion microscope

The field-ion microscope is basically a simple device. A generic form of the instrument is shown schematically in figure 13. All modern FIMS usually incorporate a cryogenically cooled specimen tip which is biased to a high positive potential, and a microchannel plate ion detector. These are located in an ultrahigh-vacuum environment that can be selectively backfilled to about $10^{-5}$ Torr (1.33 kPa) with a very pure imaging gas. Since helium or neon are frequently used for imaging, a liquid nitrogen cooled, titanium sublimator provides effective pumping of all background contaminants during the imaging process. If helium is used for imaging, it can be conveniently introduced into the vacuum chamber by diffusion through the very thin walls of an electrically heated quartz or Vycor thimble (Müller and Tsong 1969). The diffusion process obviates the need for a very pure helium supply since impurities in the gas cannot diffuse into the vacuum system.

A fibre optic faceplate coated with a fluorescent material (such as manganese-doped zinc orthosilicate) can be used to conveniently record the field-ion image. The faceplate transmits the image to laboratory ambient where it can be easily photographed by directly contacting the faceplate with a photographic emulsion. If Polaroid type 55 film is used, a print and a negative can be immediately obtained without the need for darkroom facilities (Panitz 1973). Since lenses are not used, the system is inherently fast and distortion free. In many instances images can even be recorded without the use of a channel plate (Hren and Newman 1967).

One disadvantage of a simple FIM is the relatively long time required to change specimen tips, particularly if ultrahigh-vacuum conditions must be re-established prior to imaging. In order to overcome this difficulty, the tip can be placed in a prepumped specimen chamber and transferred under vacuum, through an isolation valve, to the base of the cryogenic reservoir. Alternatively, a multiple tip holder can be employed so that ten or fifteen tips can be inserted into the vacuum chamber at one time, with each tip individually selectable for imaging (Khoshnevisan and Stephan 1973). This approach has been used in the author's laboratory for many years.

Methods for introducing a number of very pure imaging gases, for heating the tip, changing its orientation in space, and cooling the tip below 60 K (in order to improve image resolution) introduce additional complexity. As with most instruments, universality in an FIM is usually expensive and generally involves compromise. Whereas the simple FIM of figure 13 would cost less than $20 000 (US) to construct, an FIM with a full complement of features (including a mass spectrometer to identify field-desorbed species) could easily cost more than a quarter of a million dollars. Although the complexity of a sophisticated FIM is comparable to that of more conventional surface analytical instruments, it differs from these instruments in that it must be constructed and assembled by the individual investigator, a process which requires time and experience. Currently, no commercial field-ion microscopes are being produced, although at least one large manufacturer of vacuum equipment (Vacuum Generators, England) will assemble custom-built instruments on an individual basis.

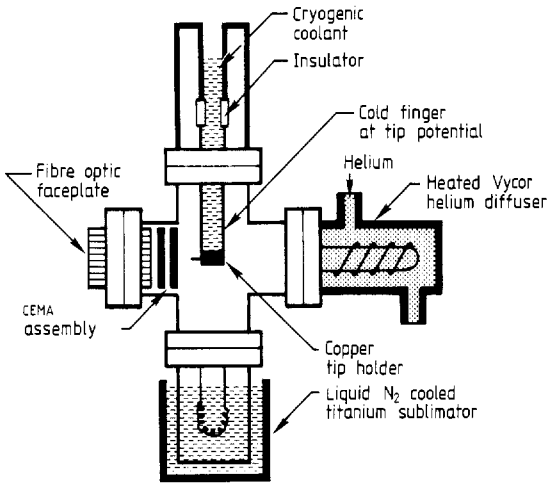


**Figure 13.** A schematic drawing of a simple, generic form of a modern field-ion microscope. The device is typically constructed from interchangeable, stainless steel vacuum components. The chamber is attached to a conventional ultrahigh-vacuum system which is not shown. With a simple FIM, metallic surfaces can be imaged with atomic resolution, and surface processes directly examined as a function of surface crystallography and morphology.

## 12. The atom-probe FIM

Although the simplest FIM can provide information about the arrangement of lattice atoms exposed at the surface of a specimen tip, even the most complicated FIM cannot provide reliable information on their chemical identity. Furthermore, since certain adsorbates (such as hydrogen) are invisible in an FIM image the cleanliness of the surface cannot be documented by direct observation. Fortunately, the field-evaporation process provides an unambiguous method to identify the species which form the surface of the tip. The ions which are produced can be directed into a mass spectrometer and their identity determined from their mass-to-charge ratio. Even the identity of a single field-evaporated atom can be determined, providing what has become the ultimate microanalytical capability – an 'atom-probe' (Müller and Panitz 1967).

In order to obtain a sufficient signal-to-noise ratio to detect one ion and have the capability of identifying species over an extended mass range, Barofsky suggested what has become the most common type of atom-probe, the time-of-flight or TOF instrument†. In the TOF atom-probe, a voltage pulse of a few nanoseconds duration, applied to the tip, serves to limit the field-evaporation process to a very short time duration. Using the leading edge of the pulse as a zero-time marker, the travel time of successive field-evaporated species to a detector can be measured. From the known kinetic energy of the ions (determined by the total potential applied to the tip), and the measured flight distance, the identity of each field-evaporated species is determined. By using a small 'probe hole' as the entrance aperture to the spectrometer, its field-of-view can be limited to a preselected field-evaporation site on the tip surface. In order to sample the entire tip surface, the tip is mounted into a gimbal system so that it can be moved in space about its apex. In this way an FIM image of the surface can be swept over the entrance to the spectrometer until a selected surface site is aligned with the probe hole. In effect, the atom-probe can '... determine the nature of one single atom seen on a metal surface and selected from neighbouring atoms at the discretion of the observer' (Müller *et al* 1968).

Several variations of the TOF atom-probe have appeared since its introduction in 1968, including the use of a magnetic sector spectrometer (Müller and Sakurai 1974) and time gating in order to produce elemental maps of the entire tip surface (Panitz 1974, 1978). A recent development involves the use of a short-duration thermal pulse from a laser (rather than a voltage pulse) to initiate field-desorption at a constant field strength (Nishigaki *et al* 1979, Kellogg and Tsong 1980). The advantages of this approach are just being realised. Since it is not necessary to transmit nanosecond duration voltage pulses to the tip apex, materials such as very pure silicon which have a high intrinsic resistance can be analysed (Kellogg and Tsong 1980, Kellogg 1982b). By using a metal coating to establish a steady-state field at the tip apex, pure insulators such as Pyrex and quartz can also be examined (Kellogg 1982c).

The thermal and field-dependent contribution to the charge distribution of field-evaporated ions have also been independently observed for the first time with the pulsed laser atom probe (Kellogg 1981, Kellogg 1982a). Photon-induced chemistry in high fields may have been observed with such an instrument (Nishigaki *et al* 1979), and a dramatic improvement in mass resolution over the conventional TOF atom-probe are being realised (Tsong *et al* 1982). An improvement in mass resolution has always been recognised as a potential benefit of the technique (Panitz 1978) since the ion kinetic energy is only determined by the DC potential applied to the tip. In the voltage pulsed atom-probe, reflections caused by the impedance discontinuity of the tip assembly typically produce an energy spread of a few per cent in an ion's kinetic energy. This limits the effective mass resolution to $\Delta M/M \approx 200$. Although an isochronal focusing element can minimise this problem (Müller and Krishnaswamy 1974), the pulsed laser atom-probe provides a simpler and more cost effective solution.

For surface studies, the temperature increase produced during laser pulsing (typically, several hundred degrees K) may pose a problem. Although the increase in temperature can be used to study changes in tip morphology at elevated temperatures (Kellogg 1982a) it may complicate the study of adsorbate–metal interactions, particularly if surface mobility is appreciable. A principle advantage of low-temperature field-desorption over conventional thermal desorption is its ability to probe the surface at a temperature where local surface migration can be neglected (Panitz 1979).

## 13. Surface diffusion in the FIM

The ability of the FIM to observe individual metal atoms adsorbed on atomically clean and perfect crystal planes of different crystallographic orientation is a major advantage of the FIM technique. By purposely inducing the diffusion of a metallic adsorbate in the absence of a field, the FIM can provide a unique capability for probing the interatomic potentials which exist at the vacuum–surface interface. The motion of small clusters of atoms, and their sensitivity to surface morphology and adjacent adsorbates are all accessible to direct experimental observation in an FIM diffusion experiment.

† In the fall of 1966, D F Barofsky and the author were graduate students in Erwin Müller's laboratory at the Pennsylvania State University. Erwin had just returned from a European trip with the idea for an atom-probe FIM. Barofsky suggested the use of a time-of-flight mass spectrometer and performed the initial calculations which demonstrated that this approach was feasible.

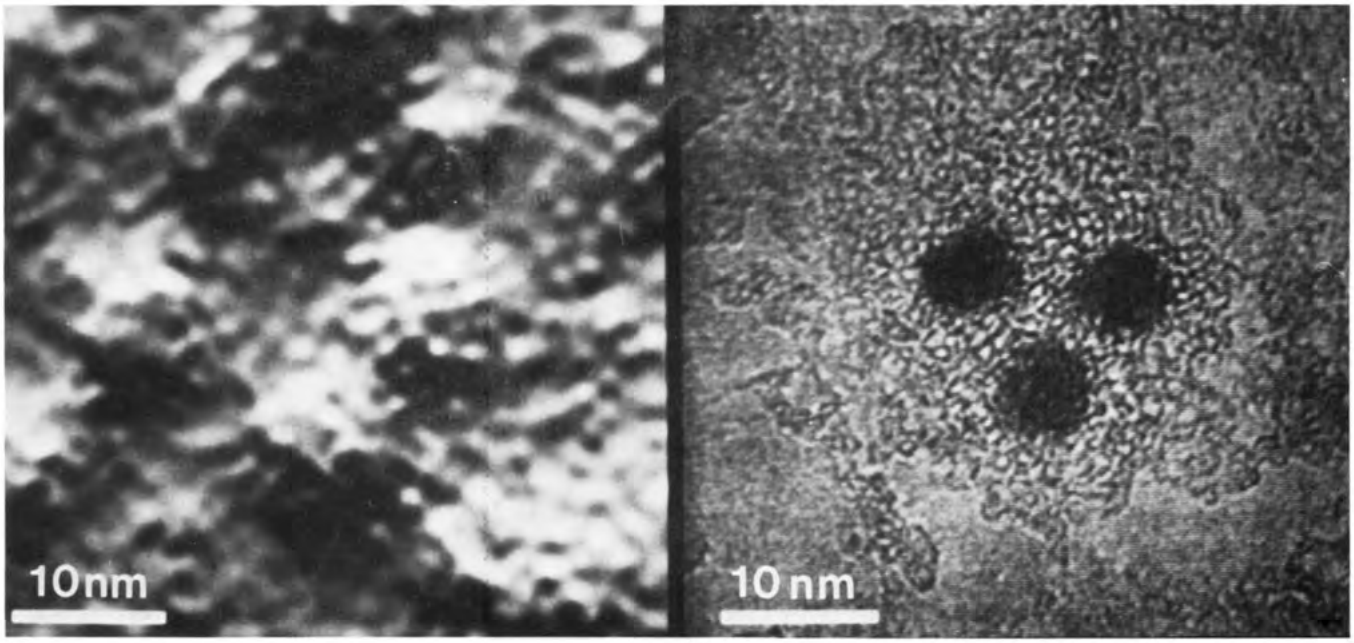


**Figure 14.** (*a*) A three-dimensional digital reconstruction of the unstained spherical protein shell of several isolated ferritin molecules deposited on to the surface of a tungsten tip. The image was created from a series of images taken during controlled field-desorption of a thick benzene layer condensed onto a molecule-coated tip surface at 20 K. The imaging process appears to be nondestructive and reproducible (see text). (*b*) A transmission electron microscope (TEM) image of the iron-rich core of three individual ferritin molecules deposited on to a very thin carbon substrate. The combination of a high concentration of iron within the molecule and a low-Z substrate, make TEM imaging of ferritin's core possible. The unstained protein shell of the molecule cannot be seen.

The first quantitative measurements of the migration of tungsten atoms on tungsten, and their binding energy were made by Ehrlich and co-workers (Ehrlich and Hudda 1966, Ehrlich and Kirk 1968). Other experiments quickly followed which were designed to investigate the motion of individual adatoms (Plummer and Rhodin 1968, Bassett and Parsely 1969a, b, 1970, Tsong 1971a, Plative and Graham 1978), adatom clusters and their dissociation (Bassett and Parsely 1969, Bassett 1970, Bassett and Tice 1973), pairs of adatoms cooperatively diffusing through a long-range interaction (Tsong 1971b, 1972, Graham and Ehrlich 1973, 1974a, b, 1975, Ayrault and Ehrlich 1974, Tsong *et al* 1975, Sakata and Nakamura 1975, Reed and Ehrlich 1975, Stolt *et al* 1976), and surface rearrangement with and without an electric field (Tsong 1972, Bassett 1975, Nishigaki and Nakamura 1976).

The procedure for performing a diffusion experiment in the FIM is straightforward. Field-evaporation is used to obtain a perfect surface morphology which is imaged in atomic resolution by low-temperature field-ion microscopy. For adatom studies, a metallic adsorbate is deposited onto the tip in the absence of the field (usually by thermal evaporation from a heated filament). If subsequent field-ion imaging shows that the adsorbate coverage is too great, field-desorption is used in order to reduce the number of adsorbed species. Eventually the correct number of adsorbates on the required crystal plane will be obtained.

Surface diffusion is initiated by heating the tip to a known temperature (usually 200–500 K) for a fixed interval of time. Generally, the field is removed during the diffusion interval, although measurements of diffusion in the presence of a field can yield information on the polarisability and the surface-induced dipole moment of an adatom (Tsong and Walko 1972, Graham and Ehrlich 1974, Tsong and Kellogg 1975, Kellogg and Tsong 1977). Following the diffusion interval, the tip is quickly cooled so that a low-temperature field-ion image can be taken of the new adatom position on the surface. The process is then repeated, often hundreds of times.

From a series of field-ion images, the mean-square displacement of an adatom can be measured as a function of diffusion temperature. A measurement accuracy approaching 0.01 nm is possible because adatom displacement can be directly compared to the known interatomic spacings on well resolved crystal planes in the FIM image. Since reliable statistics require many temperature cycles, a typical diffusion experiment can last for many hours. Ultrahigh-vacuum conditions are mandatory.

The diffusivity, $D_0$, and the activation energy for diffusion, $E_d$, can be obtained from experimentally measurable parameters by the relation

$$\langle x^2 \rangle / 2\gamma = D_0 \exp(-E_d/kT) \tag{7}$$

(see, for example, Kellogg *et al* 1978). The diffusivity, $D_0$, is related to the diffusion coefficient, $D$, by an expression of the form

$$D = D_0 \exp(-E_d/kT). \tag{8}$$

If the measured mean-square displacement of the adatom $\langle x^2 \rangle$, corresponds to a diffusion time interval $\gamma$ at a diffusion temperature, $T$, then a graph of $\langle x^2 \rangle/2$ against $1/T$, will yield a straight line of slope $-E_d/k$, and intercept $\ln D_0$. Numerous experiments have shown that activation energies range from 0.16 eV for a rhodium adatom on Rh(111), where $D_0 = 2 \times 10^{-4}$ eV (Ayrault and Ehrlich 1974); to 1.04 eV for a rhenium adatom on W(110), where $D_0 = 1.5 \times 10^{-2}$ (Bassett and Parsely 1969a, 1970). Diffusivities average about 30 mm $s^{-1}$, which is typical for a rhodium adatom on Rh(110)

where $E_d = 0.6$ eV. Complete tabulations of the results of FIM diffusion experiments appear in several excellent reviews (Kellogg *et al* 1978, Bassett 1973, Ehrlich 1977, Roberts and McKee 1978, Tsong and Cowan 1977, King 1980). A bibliography of FIM surface diffusion studies between 1951 and 1978 is included in a recent bibliography of FIM and related techniques (Thurstans and Walls 1980).

### 14. Biomolecular imaging

For at least fifteen years, attempts have been made to use the FIM to image biological molecules (Müller and Rendulic 1967, Machlin 1971, Graham *et al* 1973). Despite ingenious schemes to prevent the high field strength at BIV from desorbing molecules of interest, no reproducible images of biological species were ever obtained. Recently, a novel field-desorption imaging technique called 'field-ion tomography' has been introduced (Panitz 1982a, b). The first quasi three-dimensional, nondestructive and reproducible images of unstained protein molecules on a metal surface have been obtained.

In order for the technique to obtain a three-dimensional reconstruction of a biological molecule, the molecule is deposited from aqueous solution onto the surface of a large radius field-emitter tip (Panitz and Giaever 1981). After placing the tip in a simple FIM, a thick layer of benzene is condensed from the gas phase onto the tip surface. Since the tip is cooled to a temperature below 30 K, the molecules of interest are embedded in a frozen immobile layer which completely surrounds and covers them. The remaining benzene vapour is pumped away. By increasing the tip voltage, the benzene layer can be field-desorbed. Provided the layer covers the deposited molecules, the detector image will appear bright and relatively contrastless. However, as soon as a molecule is exposed, a dark feature will appear in the image. The contour of the dark feature reflects the contour of the molecule defined by its intersection with the remaining benzene layer.

From a series of successive contour slice images taken during the removal of the benzene layer, a series of molecular contours are obtained (Panitz 1982a). These can be digitally processed to reconstruct the molecule which produced them (Ghiglia and Flickner 1982). An example of an image of individual ferritin molecules (a spherical protein 13 nm in diameter) is shown in figure 14(*a*). This is the first image ever taken of an unstained protein molecule deposited on a metal substrate (Panitz 1982c). For comparison purposes, a transmission electron microscope image of the iron-rich core of this molecule (deposited on a carbon substrate) is shown in figure 14(*b*).

### 15. Summary and conclusions

The FIM is a very simple yet powerful device for studying the morphology of surfaces on an atomic scale. By controlled field-evaporation, the near-surface region of the emitter tip can be exposed for imaging in order to analyse bulk artefacts introduced intentionally or as the result of a given emitter treatment. When combined with a mass spectrometer, field-evaporation permits preselected surface species to be uniquely identified by their mass-to-charge ratio, and their distribution on various crystal planes charted. From adatom diffusion studies, binding energies and diffusivities can be measured, and the interatomic potential on clean single-crystal surfaces probed with subnanometer precision. The formation of adlayers, superlattices and the reconstruction of individual crystal planes can be studied in detail. By using controlled field-desorption of a condensed multilayer, biological molecules embedded in the layer can be nondestructively imaged in a quasi three-dimensional fashion. This novel type of imaging may provide a useful new way of observing the interaction of a wide variety of organic species with a metal surface, thereby greatly extending the capabilities of the most powerful microscope known to man.

### Acknowledgments

The author wishes to thank G L Kellogg and R J Walko for critically reviewing this paper upon its completion, and Pauline Parra for her patience and perseverance in preparing the manuscript in its final form.

### References

Aiferieff M E and Duke C B 1967
*J. Chem. Phys.* **46** 939

Ayrault G and Ehrlich G 1974
*J. Chem. Phys.* **60** 281

Barofsky P F and Müller E W 1968
*Surf. Sci.* **10** 177

Bassett D W 1970
*Surf. Sci.* **23** 240

Bassett D W 1973 in *Surface and Defect Properties of Solids* ed. M W Roberts and J M Thomas (London: The Chemical Society) **2** p 34

Bassett D W 1975
*Surf. Sci.* **53** 74

Bassett D W and Parsely M J 1969a
*Brit. J. Appl. Phys. (J. Phys. D)* ser. 2 **2** 13

Bassett D W and Parsely M J 1969b
*Nature* **221** 1046

Bassett D W and Parsely M J 1970
*J. Phys. D: Appl. Phys.* **3** 707

Bassett D W and Tice D R 1973
*Surf. Sci.* **40** 499

Brandon D G 1965
*Surf. Sci.* **3** 1

Brandon D G 1966a
*Brit. J. Appl. Phys.* **14** 803

Brandon D G 1966b
*Phil. Mag.* **14** 803

Dreschler M 1960 *IV Int. Kongr. Electronenmikroskopie* vol. 1 (Berlin: Springer) p 835 (also Müller E W p 820)

Ehrlich G 1977
*Surf. Sci.* **63** 422

Ehrlich G and Hudda F G 1966
*J. Chem. Phys.* **44** 1039

Ehrlich G and Kirk C G 1968
*J. Chem. Phys.* **48** 1465

Ernst N 1979
*Surf. Sci.* **87** 469

Eyring C F, Mackeown S and Millikan R A 1928
*Phys. Rev.* **31** 900

Feynman R P, Leighton R B and Sands M 1964 *The Feynman Lectures on Physics* vol. 2 (New York: Addison–Wesley) pp 4–10

Fink H W and Ehrlich G 1981
*Surf. Sci.* **110** L611

George T H 1965
*Bull. Am. Phys. Soc.* **10** 493

Ghiglia D C and Flickner M 1982
*Opt. Lett.* **7** 116

Gomer R J 1952
*J. Chem. Phys.* **20** 1772

Gomer R J 1959
*J. Chem. Phys.* **31** 341

Gomer R J and Swanson L W 1963
*J. Chem. Phys.* **38** 1613

Graham W R and Ehrlich G 1973
*Phys. Rev. Lett.* **31** 1407

Graham W R and Ehrlich G 1974a
*J. Phys. F: Metal Phys.* **4** L212

Graham W R and Ehrlich G 1974b
*Surf. Sci.* **45** 530

Graham W R and Ehrlich G 1975
*Thin Solid Films* **25** 85

Graham W R, Hutchinson F and Reed D A 1973
*J. Appl. Phys.* **44** 5155

Guerney R W 1932
*Proc. R. Soc.* **134** 137

Haydock R and Kingman D R 1980
*Phys. Rev. Lett.* **44** 1520

Hren J J and Newman R W 1967
*Rev. Sci. Instrum.* **38** 869

Inghram M G and Gomer R J 1954
*J. Chem. Phys.* **22** 1279

Inghram M G and Gomer R J 1955
*Z. Naturf.* a **109** 863

Inghram M G and Gomer R J 1956
*Z. Naturf.* a **10** 863

Jason A J 1967
*Phys. Rev.* **156** 156

Jason A J, Burns R P and Inghram M G 1965
*J. Chem. Phys.* **43** 3762

Kapar S and Müller E W 1977
*Surf. Sci.* **66** 45

Kellogg G L 1981
*Phys. Rev.* B **24** 1848

Kellogg G L 1982a
*Surf. Sci.* in press

Kellogg G L 1982b
*Appl. Surf. Sci.* **11/12** 186

Kellogg G L 1982c
*J. Appl. Phys.* in press

Kellogg G L and Tsong T T 1977
*Surf. Sci.* **62** 343

Kellogg G L and Tsong T T 1980
*J. Appl. Phys.* **51** 1184

Kellogg G L and Tsong T T 1981
*Surf. Sci. Lett.* **110** L599

Kellogg G L, Tsong T T and Cowan P 1978
*Surf. Sci.* **70** 485

Khoshnevisan M and Stephan C H 1973
*J. Phys. E: Sci. Instrum.* **6** 10

King D A 1980
*J. Vac. Sci. Technol.* **17** 241

Krishnaswamy S V and Müller E W 1977
*Z. Phys. Chem. N F* **104** 121

Lampton M 1981
*Sci. Am.* **245** 62

Lanczos C Z 1931
*Physik* **68** 204

Machlin E S 1971 unpublished abstracts of the *18th International Field Emission Symposium, Eindhoven, The Netherlands* p 84

Melmed A J and Stein R J 1975
*Surf. Sci.* **49** 645

Melmed A J, Tung R T, Graham W R and Smith G D W 1979
*Phys. Rev. Lett.* **43** 1521

McKinstry D 1972
*Surf. Sci.* **29** 37

Müller E W 1936a
*Z. Tech. Phys.* **17** 412

Müller E W 1936b
*Z. Phys.* **37** 838 (also **102** 734)

Müller E W 1941
*Naturwissenschaften* **29** 533

Müller E W 1951
*Z. Phys.* **131** 13

Müller E W 1956a
*Z. Naturf.* a **11** 87

Müller E W 1956b
*J. Appl. Phys.* **27** 474

Müller E W 1956c
*Phys. Rev.* **102** 618

Müller E W 1960 *Advances in Electronics and Electron Physics* **13** (New York: Academic Press) p 144

Müller E W 1965
*Science* **149** 591

Müller E W and Bahadur K 1955
*Phys. Rev.* **99** 1651

Müller E W and Bahadur K 1956
*Phys. Rev.* **102** 624

Müller E W and Krishnaswamy S V 1973
*Surf. Sci.* **36** 29

Müller E W and Krishnaswamy S V 1974
*Rev. Sci. Instrum.* **45** 1053

Müller E W and Krishnaswamy S V 1976
*Phys. Rev. Lett.* **37** 1011

Müller E W, McLane S B and Panitz J A 1969
*Surf. Sci.* **17** 430

Müller E W and Panitz J A 1967 unpublished abstracts of the *14th International Field-Emission Symposium, The National Bureau of Standards, Washington, DC*

Müller E W, Panitz J A and McLane S B 1968
*Rev. Sci. Instrum.* **39** 83

Müller E W and Rendulic K D 1967
*Science* **156** 961

Müller E W and Sakurai T 1974
*J. Vac. Sci. Technol.* **11** 878

Müller E W and Tsong T T 1969 *Field-Ion Microscopy: Principles and Applications* (New York: Elsevier)

Müller E W and Tsong T T 1973 *Progress in Surface Science* ed. S G Davison (New York: Pergamon) vol. 4 p 51

Nishigaki S, Drachsel W and Block J H 1979
*Surf. Sci.* **87** 389

Nishigaki S and Nakamura S 1976
*J. Appl. Phys. (Japan)* **15** 19

Oppenheimer J R 1928
*Phys. Rev.* **31** 67

Panitz J A 1973
*Rev. Sci. Instrum.* **44** 1034

Panitz J A 1974
*J. Vac. Sci. Technol.* **11** 206

Panitz J A 1975a
*Crit. Rev. Solid State Sci.* **5** 153

Panitz J A 1975b
*J. Vac. Sci. Technol.* **12** 210

Panitz J A 1978 *Progress in Surface Science* ed. S G Davison (New York: Pergamon) vol. 8 p 261

Panitz J A 1979
*J. Vac. Sci. Technol.* **16** 868

Panitz J A 1982a
*J. Microscopy* **125** 3

Panitz J A 1982b
*Ultramicroscopy* **7** 3

Panitz J A 1982c
*J. Microscopy* in press

Panitz J A and Foesch J A 1976
*Rev. Sci. Instrum.* **47** 44

Panitz J A and Giaever I 1981
*Ultramicroscopy* **6** 3

Plative P G and Graham W R 1978
*Thin Solid Films* **51** 175

Plummer E W and Rhodin T N 1968
*J. Chem. Phys.* **49** 3479

Reed P A and Ehrlich G 1975
*Phil. Mag.* **32** 1095

Roberts M W and Mckee C S 1978 *Chemistry of the Metal-Gas Interface* (Oxford: Clarendon)

Sakata T and Nakamura S 1975
*Surf. Sci.* **51** 313

Stolt K, Graham W R and Ehrlich G 1976
*J. Chem. Phys.* **65** 3206

Swanson L W and Gomer R J 1963
*J. Chem. Phys.* **29** 2813

Thurstans R E and Walls J M 1980 *Field-Ion Microscopy and Related Techniques: A Bibliography 1951–1978* (Birmingham: Warwick Publishing) p 123

Tsong T T 1968
*Surf. Sci.* **10** 102

Tsong T T 1971a
*J. Chem. Phys.* **54** 4205

Tsong T T 1971b
*J. Chem. Phys.* **55** 4658

Tsong T T 1972
*Phys. Rev.* B **6** 417

Tsong T T and Casanova R 1981
*Phys. Rev. Lett* **47** 113

Tsong T T and Cowan P 1977 in *Chemistry and Physics of Solid Surfaces* ed. R Vanselow (Florida: CRC Press) vol. 2 p 209

Tsong T T, Cowan P and Kellogg G L 1975
*Thin Solid Films* **25** 97

Tsong T T and Kellogg G L 1975
*Phys. Rev.* B **12** 1343

Tsong T T, McLane S B and Kinkus T J 1982
*Rev. Sci. Instrum.* in press

Tsong T T and Müller E W 1964
*J. Chem. Phys.* **41** 3279

Tsong T T and Müller E W 1970
*Phys. Status Solidi* (a) **1** 513

Tsong T T and Walko R J 1972
*Phys. Status Solidi* (a) **12** 111

Tung R T, Graham W R and Melmed A J 1982
*Surf. Sci.* **115** 576

Turner P J, Cartwright P, Southon M J, Van Oostrom A and Manley B W 1969
*J. Phys. E: Sci. Instrum.* **2** 731

Walko R J 1982 Sandia National Laboratories, Albuquerque, NM (unpublished FIM micrographs of pyrex tips formed from microcapillaries of this material)

Walko R J and Müller E W 1972
*Phys. Status Solidi* (a) **9** K9

**Dr John A Panitz** has been a member of the Technical Staff at Sandia National Laboratories, Albuquerque, New Mexico for 12 years. He worked with the late E W Müller on the development of the Atom-Probe field-ion microscope and in 1975 he patented the Imaging Atom-Probe field-ion microscope (US Patent 3 868 507). He is the author of over eighty scientific publications, review articles and book chapters relating to phenomena which occur in high electric fields. His current research interests include electrical breakdown phenomena, studies of the vacuum–solid interface using high-field analytical techniques, and the development of a novel field-ion tomographic microscope to image unstained organic and biological molecules.

Dr Panitz is a member of the American Physical Society, the American Chemical Society, the American Association for the Advancement of Science, the New York Academy of Sciences, Pi Eta Sigma and Sigma Pi Sigma.